Molecular Dynamics Simulation of Electrolyte Solutions in Ambient and Supercritical Water. 1. Ion Solvation

ARTICLE *in* THE JOURNAL OF PHYSICAL CHEMISTRY · FEBRUARY 1996

Impact Factor: 2.78 · DOI: 10.1021/jp952194o

3 AUTHORS, INCLUDING:

Perla B. Balbuena
Texas A&M University
245 PUBLICATIONS **5,740** CITATIONS

SEE PROFILE

Molecular Dynamics Simulation of Electrolyte Solutions in Ambient and Supercritical Water. 1. Ion Solvation

Perla B. Balbuena,*,† Keith P. Johnston,*,† and Peter J. Rossky*,‡

Department of Chemical Engineering and Department of Chemistry and Biochemistry, The University of Texas at Austin, Austin, Texas 78712

Received: August 1, 1995; In Final Form: November 25, 1995[⊗]

Free energies of solvation for Cl^-, OH^-, Na^+, HCl, and H_2O are calculated at ambient conditions and several supercritical water (SCW) states using molecular dynamics−free energy perturbation computer simulation. From ambient to SCW, the magnitude of reductions in the coordination number, number of hydrogen bonds, and other specific interactions are in the opposite order of the solute−water interaction energies, which are, from strongest to weakest, $Na^+ > OH^- > Cl^- > H_2O >$ HCl. This trend also applies to the magnitude of the solvation free energy, although the changes for Na^+ are very small, from ambient conditions all the way to 673 K and 0.087 g/cm^3. Bivalent cations exhibit a well-defined second shell that remains at supercritical conditions. Modest discrepancies are observed between simulation and experiment both for the local density of water about Sr^{2+} and for the free energy of solvation of NaCl, illustrating the challenges to both theory and experiment.

1. Introduction

Although aqueous solutions of electrolytes have been the subject of extensive experimental and theoretical studies up to 100 °C,[1−4] relatively little work has been done at higher temperatures. Recently, there has been great interest in supercritical water (SCW) (T_c = 647.13 K, ρ_c = 0.322 g/cm^3, P_c = 220.55 bar) solutions[5,6] motivated by the development of new technologies,[7,8] including hydrothermal oxidation of chemical wastes and hydrothermal synthesis. The design of SCW processes presents challenges due to corrosion, salt precipitation, and the extreme conditions of temperature and pressure. A fundamental understanding of ion solvation at elevated temperatures would be beneficial for modeling many chemical properties including phase behavior, salt solubilities, corrosion, dissociation of acids, bases, and salts, and proton transfer and charge transfer reactions. Ion solvation is arguably the key property for understanding the metamorphosis of water as it acquires "nonaqueous" character at high temperatures and low densities.

Much of the early knowledge concerning ion solvation in supercritical water came from macroscopic experimental measurements, e.g., calorimetry,[9] conductivity,[10] and emf measurements.[11] An extensive compilation of properties (partial molar volumes, entropies, enthalpies, and Gibbs free energies of formation of electrolytes including salts, acids, and bases in aqueous solutions) has been reported and correlated with semiempirical models based on the Born equation.[12−16] Estimations of radii for several ions in high-temperature water were also presented by Helgeson.[16] Pitzer[17,18] compiled from several publications a list of experimental solvation free energies for undissociated NaCl in steam over a wide range of temperatures and pressures.

In order to obtain free energies for dissociated ions from those corresponding to salts, acids, and bases in the associated state, it is necessary to use extrathermodynamic assumptions.[1] In ambient water (AW), single-ion solvation free energies have been obtained in this manner from electric potential differences (emf) and calorimetric measurements.[19] In SCW, single-ion free energies, enthalpies, and entropies were estimated for Na^+ and Cl^- with a semicontinuum model.[17,20] The model uses gas-phase mass spectrometry data for the hydration equilibria of Cl^- and Na^+ in ion−water clusters along with the Born model[21] for the electrostatic interactions. A related model[22] indicates that hydrogen bonding of water to these ion−water clusters stabilizes the clusters (relative to the ideal gas state), which is the opposite result of the model of Tanger and Pitzer. An alternative approach is to modify the Born model to include solvent compressibility effects.[23,24]

Solvation free energies may also be calculated based on numerical solutions to the Poisson−Boltzmann equation.[25,26] Recently, this approach has been extended to SCW to obtain free energies of solvation and activation energies[27] and also to model the S_N2 reaction of Cl^- and CH_3Cl.[28] The results are in reasonable agreement with simulation[29−31] at high and low densities, but deviations are present in the mid-density region where clustering (electrostriction) is most prevalent.

Molecular level studies of ion solvation in SCW are only just beginning. Molecular simulation has been employed for studies of pure water over a wide range of temperature and pressure.[32−36] The radial distribution functions for water about several polar, nonpolar, and ionic solutes[37−41] and ion pairing[42,43] have been investigated. Extreme conditions (e.g., a reduced density of 0.05 at the critical temperature) were found to be necessary to remove half of the water molecules in the first solvation shell about the chloride ion.[31] Thermodynamic properties have been calculated from simulation and analyzed in terms of structural properties. In the S_N2 charge transfer reaction of Cl^- and CH_3Cl,[29−31] the combined effects of changes in temperature and solvation lead to an increase in the rate constant by 9−12 orders of magnitude in SCW relative to AW. An equally large effect takes place in acid−base equilibrium, as demonstrated in the following paper in this issue.

Our objective is to simulate the free energy of solvation of representative single ions in SCW for the first time and to analyze the results in terms of the ion−water distribution functions. The Helmholtz free energies of solvation for anions

* To whom correspondence should be addressed.
† Department of Chemical Engineering.
‡ Department of Chemistry and Biochemistry.
[⊗] Abstract published in *Advance ACS Abstracts,* January 15, 1996.

0022-3654/96/20100-2706$12.00/0

(OH^- and Cl^-), a cation (Na^+), and neutral molecules (H_2O and HCl) are calculated from a combined molecular dynamics (MD)−free energy perturbation (FEP) approach[44,45] at infinite dilution in ambient water (298 K) and at several SCW states of temperature and solvent density. Water is described with the rigid simple point charge SPC/E model[46] with critical properties ($T_c = 640$ K, $\rho_c = 0.29$ g/cm^3, and $P_c = 160$ bar) estimated by simulations of Guissani and Guillot.[33] The experimental critical properties are very similar: $T_c = 647.13$ K, $\rho_c = 0.322$ g/cm^3, and $P_c = 220.55$ bar. Solute−water site−site interactions are represented by a combination of Coulombic and Lennard-Jones (LJ) pair potentials. We first discuss thermodynamic issues and theoretical methodology and then describe our results. We analyze the structural information in terms of solute−water radial pair density and pair energy distribution functions for various cations and anions. For cations, we relate the radial distribution function to recent experimental measurements in SCW.[47] Coordination numbers and the number of solute−water H bonds for the anions are also calculated for several conditions of density and temperature. Following Pitzer's approach,[20] the reduction in the absolute value of ΔA of hydration from AW to SCW is discussed in terms of the differences of solvation observed in the primary and successive shells of water and compared to previous results from semicontinuum models.[20,22] Calculated values for the free energy of solvation of Na^+Cl^- in SCW are obtained from the simulation of the individual ions and compared to experimental values.

2. Definitions of Solvation Processes

In this work we define the process of solvation as the change in Helmholtz free energy $A(T,V)$ needed to take one solute (S) particle from the ideal gas phase at constant T to a solution at the same T, keeping the density (N_S/V) constant. Thus, the Helmholtz free energy of solvation ΔA_S^{solv} is calculated[48] as the difference between the solute chemical potentials in the liquid and ideal gas phases respectively, i.e.,

$$\Delta A_S^{solv} = \mu_S^l - \mu_S^g \tag{1}$$

where μ_S^α is the change in free energy associated with inserting a particle S in phase α at a fixed position $\mathbf{R}_0$, i.e.,

$$\mu_S^\alpha = A(T,V,N_{S+1},N_W,\mathbf{R}_0) - A(T,V,N_S,N_W) \tag{2}$$

In this work ΔA_S^{solv} (eq 1) is calculated by a free energy perturbation technique[45] in which an infinitely dilute solution of S (in this case $N_{S+1} = 1$) is gradually transformed to pure solvent ($N_S = 0$). Here the standard states for the process of solvation are the ideal gas for the gas phase and the ideal solution of the same density for the liquid phase. This solvation process is sometimes referred to as the ρ process.[48] This choice of standard states is the same as the one defined by the Born model[21] of ion solvation. As discussed by Friedman,[2] the change in free energy for such a model corresponds to the difference in the work needed to charge a particle in a box of volume V filled with the solvent and the equivalent work to charge the particle in vacuum at constant volume. Corrections are needed[49] when the charging process is done under conditions of variable volume.

Experimental free energies of solvation are usually based on measurements at constant temperature and pressure; hence, they are Gibbs free energies, ΔG_S^{solv}. The reference states are sometimes different than the ones we have chosen in this study. Thus, we need to establish the necessary conversions in each case. These conversions were discussed in great detail by Ben-Naim,[48] but it is useful to include them here for clarity. For example, if the standard states are the ideal gas at 1 atm and temperature T and the hypothetical dilute−ideal solution extrapolated to a solute mole fraction $x_S = 1$, ΔG_{S-x}^{solv} (we indicate S−x to characterize this process) is related to ΔG_S^{solv} by

$$\Delta G_{S-x}^{solv} = \Delta G_S^{solv} + kT \ln(\varrho_W^l kT) \tag{3}$$

where ρ_w^l is the solvent liquid density. Another common choice of standard states is the combination of ideal gas for the gas phase and a 1 m ideal solution for the liquid phase. Here ΔG_{S-m}^{solv} is related to ΔG_S^{solv} in the ρ process by

$$\Delta G_{S-m}^{solv} = \Delta G_S^{solv} + kT \ln\left(\frac{M_W \varrho_W^l kT}{1000}\right) \tag{4}$$

where M_w is the molecular weight of the solvent.

Thermodynamics provides the relationship between the property $\Delta A_S^{solv}(T, V)$ calculated in this work and the corresponding $\Delta G_S^{solv}(T, P)$:

$$\Delta G_S^{solv} = \Delta A_S^{solv} + P\Delta V_S^{solv} \tag{5}$$

For most solutes, the term ΔV_S^{solv} is usually negligible when the solvent is water at ambient conditions. However, at other conditions where the solvent is compressible, the volume change needs to be included in the calculation.

3. Method

The free energy of solvation may be calculated with the free energy perturbation method. Chemical mutations X → Y where component X, present at infinitely dilute solution, is completely transformed to component Y are performed using molecular dynamics simulations combined with statistical−mechanical perturbation theory,[44,45] yielding free energies of hydration for the final state relative to the initial state. The free energy calculations for the mutation X(λ=0) → Y(λ=1) are done along a "reaction coordinate" represented by the parameter λ that is increased in small increments $\delta\lambda$ from the initial ($\lambda = 0$) to the final ($\lambda = 1$) state. The value of the subinterval $\delta\lambda$ depends on each particular case, since the two end points of the subinterval must be sufficiently similar for δA to converge. For each value of $\delta\lambda$, the mutation X(λ) → Y($\lambda+\delta\lambda$) is performed with force-field parameters dependent on the particular value of λ. From simulation results, the change in Helmholtz free energy δA for the subinterval is obtained:

$$\delta A(\lambda) = -kT \ln\langle \exp[-(U_{SW}(\lambda + \delta\lambda) - U_{SW}(\lambda))/kT]\rangle_\lambda \tag{6}$$

Here $\delta A(\lambda)$ is the change in free energy when the system is perturbed from λ to $\lambda + \delta\lambda$. U_{SW} is the solute−water configurational energy that depends parametrically on λ, and the brackets indicate an average taken for the solution at fixed λ. The variation of intermolecular parameters is usually described by a function linear in λ; i.e., for any atom or site i the partial charge is

$$q_i(\lambda) = (1 - \lambda)q_i|_{\lambda=0} + \lambda q_i|_{\lambda=1} \tag{7}$$

For any nonbonded pair i and j, the LJ parameters are

$$\sigma_{ij}(\lambda) = (1 - \lambda)\sigma_{ij}|_{\lambda=0} + \lambda\sigma_{ij}|_{\lambda=1} \tag{8}$$

and

$$\epsilon_{ij}(\lambda) = (1 - \lambda)\epsilon_{ij}|_{\lambda=0} + \lambda\epsilon_{ij}|_{\lambda=1} \tag{9}$$

The mutation X → nothing results in an "absolute" free energy of hydration for solute X, according to the solvation process in eq 1. Turning off the solute−solvent interactions is the same as transferring the solute into the gas phase. Each simulation representing a "disappearance" of one species is performed sequentially in two steps. In the first step, an electrostatic change in free energy for the process $X^- \rightarrow X$ is computed by gradually changing the value of λ. Note that this is applicable not only to an ionic species but also to dipoles, quadrupoles, or any species bearing a charge distribution. In the second step, for which the initial state is the uncharged molecule or atom (X) resulting from step 1, the LJ parameters are decreased as a function of λ while one or more bonds are shortened to a minimum value (about 0.2 Å). This second step, which approximates the process X → nothing, yields a van der Waals change in free energy. Due to gradual reaccommodation of the solvent molecules, this step converges more slowly. Of course, changing the sequence of steps can result in different values for the individual contributions;[50] hence, this information must be considered when comparing values from different simulations. We use a total of five subintervals $\delta\lambda$ to compute the electrostatic contribution (step 1) and from 15 to 20 subintervals for the van der Waals term.

The following tests are implemented to check the accuracy of the free energy simulations:

$$\delta A_{\lambda_i \rightarrow \lambda_{i+1}} \cong -\delta A_{\lambda_{i+1} \rightarrow \lambda_i} \tag{10}$$

and, for small $\delta\lambda$,

$$\delta A_{\lambda_i \rightarrow \lambda_i + n\delta\lambda} \cong n\delta A_{\lambda_i \rightarrow \lambda_i + \delta\lambda} \tag{11}$$

The simulations are performed in a cubic box containing 500 water molecules, and one solute molecule is held fixed at a given position. The NVT ensemble is obtained through constant temperature molecular dynamics. The temperature is reset every 250 steps through a velocity rescaling, and the time step used is 2 fs. The volume is obtained by adjusting the box size to give the desired water density while maintaining a constant number of molecules. The initial equilibration period at ambient conditions is 40 ps, whereas the equilibrations in the free energy simulations at each value of $\delta\lambda$ last about 10 ps, followed by a perturbation run of 5−10 ps. To obtain the supercritical (high-temperature and low-density) states, the box is heated to the desired temperature in intervals of about 50 K, starting from 298 K, at the ambient water liquid density, with an equilibration time of about 5 ps at each of these intermediate temperatures, followed by a volume increase made in several steps. The long-ranged forces are computed by an Ewald sum.[51,52] The average error calculated as the difference between the forward and the backward calculations (for λ from 0 to 1 and then 1 to 0) is ±0.5 kcal/mol.[53] In addition, we have evaluated standard deviations in the incremental free energy differences using the method of batch means.[54] The average error of the incremental free energy differences is 0.1 kcal/mol. Simulations were performed at ambient conditions (298.15 K and 0.997 g/cm^3) and at three supercritical water states. The first on the model critical isochore (ρ = 0.29 g/cm^3) at T = 673.15 K (1.05 times the model critical temperature), the second at a density 3 times lower than the critical (ρ = 0.087 g/cm^3) and T = 673.15, and the third on the critical isochore (ρ = 0.29 g/cm^3) and T = 768.15 K (1.2 times the model critical temperature).

4. Models and Parameters

Table 1 shows the charges, bond lengths, angles, and LJ parameters used for each of the solutes. In most cases, the selected LJ parameters for the ion−water interactions have been reported to give good agreement with experimental free energies of solvation in AW. In the SPC/E model, the water molecule is a LJ sphere with the oxygen atom in its center. Each hydrogen atom is separated by 1 Å from the oxygen, and the bond angle is 109.47°. The atomic charges (−0.8476e for oxygen and 0.4238e for hydrogen) are slightly larger than those given by the original SPC model[55] to include a mean field polarization effect. The site−site interactions have Coulombic and LJ terms (σ_{00} = 3.166 Å and ϵ_{00} = 0.65 kJ/mol; σ_{HH} and ϵ_{HH} are taken as zero):

TABLE 1: Charges and Lennard-Jones Parameters Used in the MD Simulations

ion/ molecule	site	q_i (e)	σ_{iw} (Å)	ϵ_{iw} (kJ/mol)	bonds/angles	ref
OH^-	O	−1.3	3.233	0.632	R(OH) = 0.953 Å	74
	H	0.3	2.083	0.231		
Cl^-	Cl	−1	3.791	0.566		75
HCl	H	0.18	0	0	R(HCl) = 1.275 Å	76
	Cl	−0.18	4.062	0.566		
H_2O	O	−0.8476	3.166	0.65	R(OH) = 1 Å	46
	H	0.4238	0	0	∠HOH = 109.47°	
Na^+	Na	1	2.69	0.5144		77
K^+	K	1	3.952	0.0299		57
Rb^+	Rb	1	4.218	0.0216		57
Ca^{2+}	Ca	2	2.763	1.107		57
Sr^{2+}	Sr	2	3.134	0.567		57

$$u_{WW}(r_{12}) = \sum_{\alpha=1}^{3}\sum_{\beta=1}^{3} \frac{q_1^{\alpha} q_2^{\beta}}{r_{12}^{\alpha\beta}} + 4\epsilon_{OO}\left[\left(\frac{\sigma_{OO}}{r_{OO}}\right)^{12} - \left(\frac{\sigma_{OO}}{r_{OO}}\right)^{6}\right] \tag{12}$$

For the solute−water interactions, the potential has a similar combination of Coulombic and LJ terms:

$$u_{SW} = \sum_{\beta=1}^{3} \frac{q^S q_\beta^W}{r_{S\beta}} + 4\epsilon_{SO}\left[\left(\frac{\sigma_{SO}}{r_{SO}}\right)^{12} - \left(\frac{\sigma_{SO}}{r_{SO}}\right)^{6}\right] \tag{13}$$

Although the technology exists for including quantum mechanical effects on the solvent distribution, and the SPC/E model should be a relatively accurate one for this purpose,[56] the effects are expected to be quite small even at ambient temperature,[56] so that the extra computational effort involved is not warranted in this study.

5. Results and Discussion

5.1. Solute−Water Pair Distribution Functions. *5.1.1. Anions.* In order to quantify solvation in the first shell near the solute in contrast to the bulk, we calculated, as in previous work,[30,31] the local density $\rho_{XY}(r)$ in g/cm^3, defined as the product of the pair radial distribution function $g_{XY}(r)$ times the bulk density, where X is the solute site and Y is one of the water sites (O or H). We present this sequence for various $\rho_{XO}(r)$, starting with $\rho_{OO}(r)$ and $\rho_{HO}(r)$ for OH^- (Figure 1a,b). Note that the first index (in this case, O or H) represents a site on the anion, while the second index (O) refers to the oxygen belonging to a water molecule. In AW (Figure 1a) there is a very well-defined structure surrounding the oxygen site of OH^-. The first peak is sharp and centered at 3 Å and gives a maximum value of about 5.5 g/cm^3, more than 5 times the AW bulk density. The second layer is also well-defined, and the maximum local density in that layer is about 1.5 g/cm^3. The structure changes at supercritical conditions; however, the first shell remains very well defined, with a slightly broader peak yielding a maximum value of about 2.5−2.8 g/cm^3, which

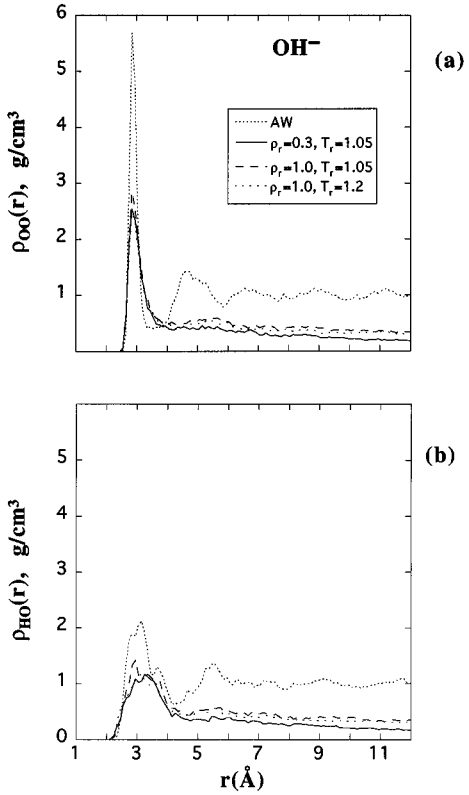

Figure 1. Spherically averaged site−site solute−water local density distribution functions for OH^- in AW and SCW: (a) oxygen (anion)−oxygen (water); (b) hydrogen (anion)−oxygen (water).

represents an increase of 10 (at $\rho_r = 1.0$) to 28 (at $\rho_r = 0.3$) times the respective bulk densities (0.29 and 0.087 g/cm^3). An increase of 14% in the reduced temperature does not change solvation significantly in the first shell. The persistence of the first shell at high temperatures and low densities is due to the solute−water interactions, which are much stronger than water−water interactions.

Figure 1b is the equivalent of Figure 1a for the water molecules surrounding the hydrogen atom of the OH^-. The radial distribution functions for this asymmetric anion show the effect of one site on the structure surrounding the other site; in this case, the O influences the water structure near H, and vice versa. However, the higher charge on the oxygen (Table 1) produces more attraction (and consequently more solvation) for the water molecules forming hydrogen bonds with this atom than in the case of the hydrogen. As shown by Figure 1b, there is a maximum local density of water molecules of 2 g/cm^3, i.e. twice the bulk density, in the first shell centered at about 3.2 Å, while a slightly enhanced structure compared to the bulk is observed in the second shell. At supercritical conditions, as noted for the case of ρ_{OO}, the first peak is reduced to half of its value in AW, which still represents a substantial number of molecules compared to the bulk densities. Almost no structure is seen beyond the first shell.

The solvation of the chloride ion is presented in Figure 2. In previous simulations with the SPC model, strong solvation of this anion is observed at dense supercritical states[37] as well as over a wide range of densities down to 0.014 g/cm^3 and temperatures up to 1.3 of the critical.[29−31,41] Figure 2 shows that the SPC/E model yields similar results for this case. The $\rho_{ClO}(r)$ in AW has a first sharp peak centered at about 3.2 Å and reaches a maximum of about 3.5 g/cm^3. As in the case of $\rho_{OO}(r)$ for the ion OH^- (Figure 1a), there is a well-defined structure that extends to further shells. Due to the smaller charge on Cl^- in comparison to the partial charge on O in OH^-, and

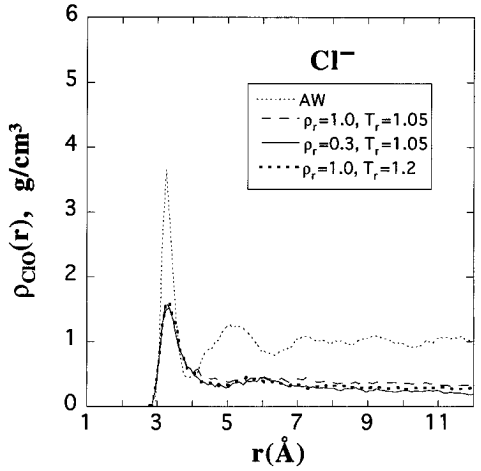

Figure 2. Same as Figure 1 for Cl^-−oxygen (water).

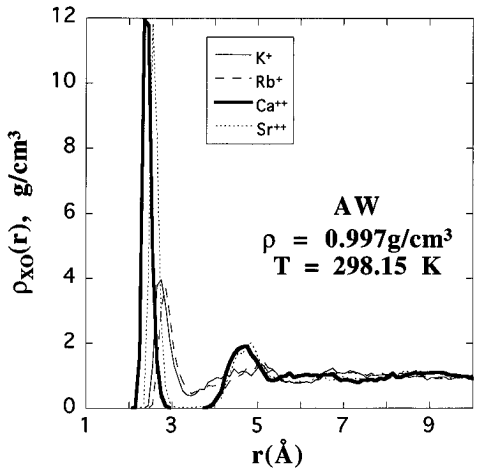

Figure 3. Spherically averaged site−site cation−oxygen (water) local density distribution functions for K^+, Rb^+, Ca^{2+}, and Sr^{2+} in AW.

also the radius difference, the local density of water near the Cl^- is lower. In SCW the first peak remains very high even at the lowest density, and the local density in the first shell near the Cl^- is enhanced from 6 to 20 times with respect to the bulk densities (0.29 and 0.087 g/cm^3) at 673.15 K. The second layer of water molecules surrounding the Cl^- is slightly more defined than in the case of OH^- (Figure 1a), indicating a relatively larger solvent ordering induced by this anion. Again, the effect of high kinetic energy causes the broadening of the first peak at supercritical conditions.

5.1.2. Cations. Figure 3 shows the local densities of water at ambient conditions surrounding two monovalent and two bivalent cations. The cation−water LJ parameters (Table 1) were taken from published data,[57] where good agreement was reported with experimental free energies of solvation in AW. Comparison of water structure near Cl^- (Figure 2) versus the monovalent cations Rb^+ and K^+ (Figure 3) indicates that the anion induces slightly more structure in the surrounding water molecules than the monovalent cations. This was reported also by Geiger[58] from MD simulations in AW. Since the distribution of charges in the water molecule is not symmetric, the partial positive charges (H^+) can approach their counterion more closely than the negative (O^-). The strong solvation of the bivalent cations is caused not only by the charge of +2 but also by the smaller radius of the solutes. In a similar study, the same effect was observed[59] by decreasing the σ(LJ) parameter on ions of the same charge.

Figure 4 depicts the corresponding local densities at a SCW condition. As noted for the anions, solvation in the first shell

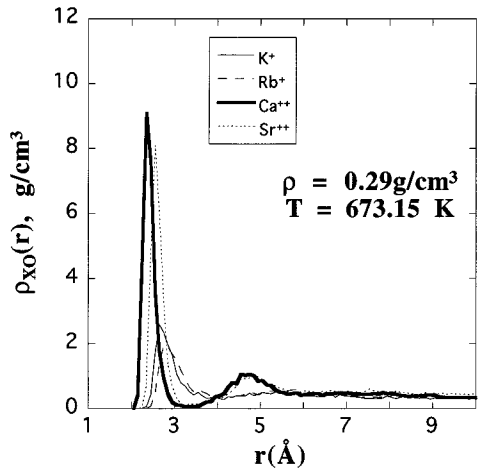

Figure 4. Same as Figure 3 for cations in SCW ($\rho = 0.29$ g/cm^3 and $T = 673.15$ K).

remains extremely high even at the lowest density state (0.087 g/cm^3) at 673.15 K (not shown). Maximum values of about 30−100 times larger than the bulk densities are observed for the local densities near Ca^{2+} and Sr^{2+}, while for K^+ and Rb^+ the enhancement is of the order of 9−20 times for densities of $\rho = 0.29$ and 0.087 g/cm^3, respectively. It is very interesting that the second shell persists in SCW for the bivalent cations, even at the lowest density, indicating a very strong ion−water interaction in the first shell reinforced by the formation of H bonds between the water molecules in the first and second shells. This characteristic of the bivalent cations, which is even stronger for the trivalent cations, has been observed by several experimental studies in AW with infrared spectroscopy[60] and neutron diffraction.[61] An interesting theoretical study on this topic based on a continuum model was presented recently.[62] One fundamental point to be investigated regarding the persistence of these shells at extreme conditions of low density and high temperature is the residence time of the water molecules in these shells. This is especially important when studying chemical reactions. Further work will be presented addressing these issues.[63]

Recently X-ray absorption measurements of solvation of Sr^{2+} (strontium nitrate and strontium oxide at a concentration of 0.2 M) were reported at ambient and supercritical conditions (658 K and pressures in the range 269−339 bar).[47] From these studies it was concluded that the density in the first solvation shell is reduced by a factor of 0.52 with respect to ambient conditions while the simulations yield a decrease of less than 1% (Table 2). Three important differences should be considered. As stated in the Introduction, these simulations consider the ideal case of an infinitely dilute solution, where ion−ion association is absent. In contrast, the experimental measurements were made at finite concentration of 0.2 M. The second important point is that the conversion of the experimental data to the reported properties (in this case radial distribution functions) requires some assumptions. Finally, the charges and LJ parameters used in the force fields have been adjusted to accurately reproduce structural and polarization properties in AW. For example, the dipole moment of an individual water molecule in the SPC/E model is artificially high. Thus, it may not be as accurate at higher temperatures, possibly leading to an overestimation of the amount of solvation. Thus, the resolution of this discrepancy will require further study.

5.1.3. Coordination Numbers and Solute−Water H Bonds. Before leaving the topic of radial distribution functions, we present in Table 2 results for the solute−water coordination number (n_{XO}) and the number of H bonds (n_{HB}), both evaluated using a geometric criterion. The coordination number was found

TABLE 2: Coordination Numbers and Number of H Bonds for Solute−Water Interactions

ion/molecule	density (g/cm^3)	T (K)	n_{XO}[a]	R (Å)	n_{HB}	R (Å)
OH^-	0.997	298	6.6	3.5	6.25	2.5
	0.290	673	7.0	4.0	5.30	2.7
	0.087	673	6.5	4.0	5.00	2.7
	0.290	768	6.6	4.0	4.85	2.7
Cl^-	0.997	673	7.4	4.0	6.70	3.0
	0.290	673	8.1	4.75	4.5	3.0
	0.087	673	7.5	4.75	4.4	3.0
	0.290	768	7.8	4.75	4.5	3.0
Na^+	0.997	298	5.2	2.95		
	0.290	673	4.5	3.05		
	0.087	673	4.6	3.05		
K^+	0.997	298	5.9	3.4		
	0.290	673	5.7	3.85		
	0.087	673	4.8	3.85		
	0.290	768	5.3	3.85		
Rb^+	0.997	298	5.5	3.4		
	0.290	673	5.5	3.85		
	0.087	673	5.3	3.85		
	0.290	768	4.6	3.85		
Ca^{2+}	0.997	298	8.0	3.0		
	0.290	673	7.2	3.2		
	0.087	673	7.1	3.2		
	0.290	768	7.0	3.2		
Sr^{2+}	0.997	298	7.9	3.0		
	0.290	673	7.3	3.2		
	0.087	673	7.4	3.2		
	0.290	768	7.4	3.2		
HCl	0.997	298	24.9	5.75		
	0.290	673	6.4	5.75		
	0.087	673	2.2	5.75		
H_2O	0.997	298	5.1	3.5	3.8	2.5
	0.290	673	3.1	4.0	1.4	2.5
	0.087	673	1.6	4.0	0.6	2.5

[a] For each polyatomic species, X is the larger atom.

by integrating $g_{XO}(r)$ from $r = 0$ to $r = R$, where R (Table 2) is the radial distance from the center of the solute X to the minimum after the first peak in $g_{XO}(r)$. A comparison of the coordination numbers at the different states for OH^- (based on the oxygen atom), Cl^-, and the cations reveals that highly solvated states persist even at the lowest density (0.087 g/cm^3) and the highest temperature (768.15 K). For comparison, we list in Table 2 the corresponding values for two neutral molecules, H_2O and HCl, at the same conditions of density and temperature. For HCl, the coordination number based on the Cl site drops from a value of about 25 in AW (note the larger value of R used for HCl compared to Cl^-) to values of 2−6 in SCW. For pure water, the coordination number decreases by 40% from AW to SCW ($\rho = 0.29$ g/cm^3, $T = 673.15$ K). The smaller reduction in solvation of ions compared to neutral molecules is due to the fact that the ion−water interactions are stronger than the molecule−water interactions, as noted in previous studies.[30,31,41]

The number of H bonds for the anion−water interactions was estimated geometrically by integrating $g_{XH}(r)$. As noted previously,[30,31,41] the number of H bonds with the anions decreases at a faster rate compared to the coordination number when temperature is increased or density is decreased. In the case of the neutral molecules, the decrease is even more drastic. For example, from AW to SCW the decrease in the number of H bonds is 20% for OH^- and 33% for Cl^-, compared to 60−80% for water at the conditions analyzed.

The reduction in the number of solute−water H bonds from AW to SCW for OH^-, Cl^-, and water will be shown to be consistent with the strength of the hydrogen bonds. The calculated solute−water pair energy distributions are displayed in Figures 5 and 6 for the anions and the neutral molecules in

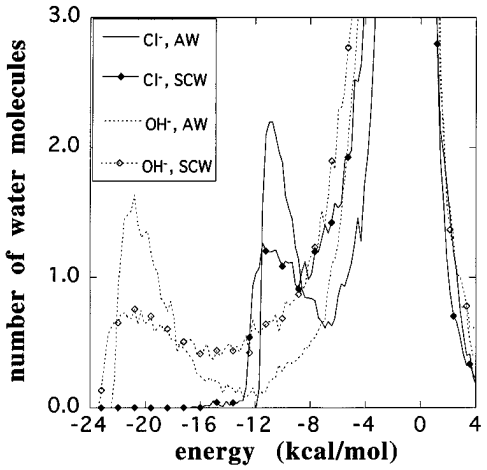

Figure 5. Solute−water pair energy distributions solute−water for anions in AW and SCW ($\rho = 0.29$ g/cm^3 and $T = 673.15$ K).

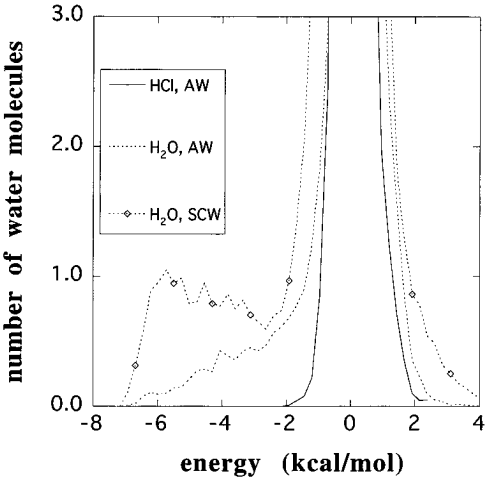

Figure 6. Same as Figure 5 for neutral molecules, H_2O and HCl.

AW and SCW ($\rho = 0.29$ g/cm^3 and $T = 673$ K). The three species forming H bonds in AW (OH^-, Cl^-, and water) display two peaks in the distribution of energies between solute−water pairs. The maximum located near zero energy corresponds to the majority of solvent molecules, which have small interaction energies due to their large distance from the solute. The other peak, much smaller in magnitude, is located in the region of negative energies and corresponds to the water molecules forming H bonds with the solute. It is centered at about −22 kcal/mol for OH^-, −10 kcal/mol for Cl^- (Figure 5), and approximately −5 kcal/mol for water (Figure 6). These energies agree with values reported by other authors in AW.[35,64,65] The pair energy distribution for HCl (Figure 6), on the other hand, does not show any significant peak. Thus, if H bonds are formed between HCl and AW, their bond energy must be defined to be low. The loss in hydrogen bonding from AW to SCW for each solute (from the geometric criterion, Table 2) is directly related to the strength of the H bond energy from the energetic criterion. In other words, more energy (higher kT) is required to break the strongest H bonds.

The distribution of energies corresponding to the interaction Na^+−water is depicted in Figure 7 for AW and two supercritical conditions. The interaction between the cation and the negatively charged oxygen in the water molecule is −22 kcal/mol. In SCW there is a broader distribution, and although the peak height decreases, the magnitude of the decrease is considerably smaller than in the case of the anions (Figure 5) even at the lowest density. Based on the energies of the respective solute−water interactions, the amount of thermal energy needed to break the first solvation shell decreases in the order $Na^+ > OH^- > Cl^- > H_2O >$ HCl. To further investigate the stability in the first solvation shell, we performed simulations at an even lower density, $\rho = 0.0145$ g/cm^3, and at a series of temperatures from 768 to 1000 K (Figure 8). The sharper decrease of the Cl^- coordination number compared to Na^+ follows its weaker interaction with water. This understanding of the microscopic behavior will play a vital role in the following analysis of the macroscopic thermodynamic properties of solvation.

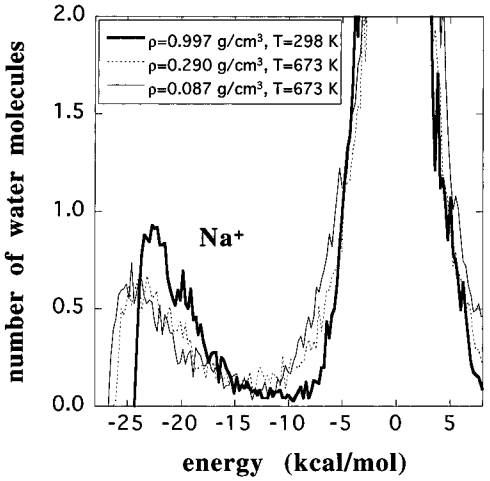

Figure 7. Same as Figures 5 and 6 for Na^+ in AW and SCW ($\rho =$ 0.29 and 0.087 g/cm^3 at $T = 673.15$ K).

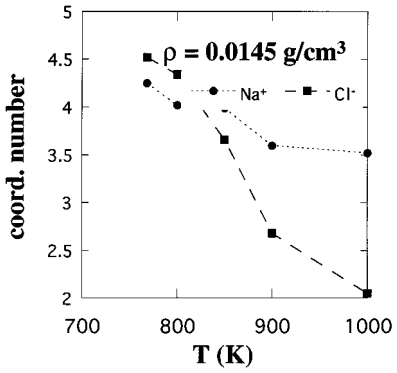

Figure 8. Effect of temperature on calculated coordination numbers in the first shell for Na^+ and Cl^- at $\rho = 0.0145$ g/cm^3.

TABLE 3: Experimental Energies of Solvation (kcal/mol) at 298.15 K

ion	ΔG^{solv}_{S-m}	ΔG^{solv}	ΔH^{solv}_{S-m}	$-T\Delta S^{solv}_{S-m}$	ref
Na^+	−72.4	−74.3	−80.2		78
	−98.2	−100	−106		19
	−89.6	−91.5			4
Cl^-	−75.8	−77.7	−81.4	5.6	19
			−85.3		66
	−75	−76.9			79
OH^-			−101		19
			−109		66
	−104	−106			79
	−90.6	−92.5	−101	10.6	2
H_2O	−4.4	−6.29			79
		−6.32			48
HCl	1.4	−0.49			79

5.2. Solvation Properties: Simulation Results and Analysis. *5.2.1. Free Energies of Solvation.* Table 3 presents a set

TABLE 4: Calculated Helmholtz Free Energies of Solvation (kcal/mol)

ion/molecule	$T = 298$ K, $\rho = 0.997$ g/cm^3	$T = 673$ K, $\rho = 0.290$ g/cm^3	$T = 673$ K, $\rho = 0.087$ g/cm^3	$T = 768$ K, $\rho = 0.290$ g/cm^3
Cl^-	−70.7	−52.2	−50.2	−48.6
OH^-	−93.3	−70.0	−62.7	−65.1
Na^+	−76.7	−73.7	−75.5	−73.7
HCl	1.18	1.94	0.67	3.17
H_2O	−8.55	−3.24	−2.06	−2.38

of experimental thermodynamic properties of solvation at 298.15 K for the solutes studied in this work. Most of the data[19,66] are from extended compilations given by Rosseinsky,[19] although other sources are also included. These data (ΔG^{solv}_{S-m}) are based on the standard state given by eq 4. The correction for differences in standard states is accomplished in the column labeled ΔG^{solv}. The original measurements were reported as values relative to the proton hydration, i.e., for an anion of charge z,

$$\Delta Y = \Delta Y_{X^-} + z\Delta Y_{H^+} \tag{14}$$

and for a cation,

$$\Delta Y = \Delta Y_{X^+} - z\Delta Y_{H^+} \tag{15}$$

where Y represents the free energy, enthalpy, or entropy of solvation of ion X. Thus, the absolute value of solvation of the ion is based on the assigned value of the corresponding property for the proton. Rosseinsky uses a value of $\Delta G_{H^+} = -260.5$ kcal/mol and $\Delta H_{H^+} = -269.7$ kcal/mol, while Rashin and Honig[66] base their calculations on $\Delta H_{H^+} = -262.18$ kcal/mol.

Table 4 displays our calculated values for ΔA^{solv} for the various species according to eq 1. For ambient water conditions ($T = 298.15$ K and $\rho = 0.997$ g/cm^3) where the term $P\Delta V^{solv}$ is negligible, the results can be compared with those in Table 3 (ΔG^{solv}). In view of the approximations involved in the estimation of experimental single-ion hydration properties, we consider the agreement between simulated and experimental data to be quite good.

The free energy of solvation can be analyzed in terms of the microscopic strengths of the specific interactions which appear in the order $Na^+ > OH^- > Cl^- > H_2O > HCl$. On the basis of the local densities and the energy distribution functions, OH^- was shown above to be better solvated than Cl^- in AW due to its smaller size and more negative partial charge. Therefore, the free energy is more negative for OH^- at all conditions. However, the reduction in the magnitude of free energy of solvation from AW to SCW is similar for the two ions.

For Na^+, the free energy changes very little from AW. This result is not observed for any of the other ions. It is a consequence of the strong cation−water interaction as seen in the pair energy distribution (Figure 7) and in the persistence of coordination number in the first shell (Figure 8).

We have also calculated (not shown) the free energies of solvation for the ionic species in Table 4 using a Born model.[21] The Born radius was adjusted to give the simulation value for the free energy in AW (Table 4). The Born model predicts reasonable solvation free energies of anions at a high SCW density ($\rho = 0.29$ g/cm^3). However, at the low SCW density, the simulation value is underpredicted, since the continuum model does not consider the local density, which is much larger than the bulk value.[28]

5.2.2. Energies and Entropies of Solvation. As has been extensively discussed and formally proven by several authors,[59,67,68] the energy and entropy of solvation can be written as

TABLE 5: Calculated Changes in Energy ΔE^{solv} and Entropy $-T\Delta S^{solv}$ (kcal/mol)

	$T = 298$ K, $\rho = 0.997$ g/cm^3		$T = 673$ K, $\rho = 0.290$ g/cm^3		$T = 673$ K, $\rho = 0.087$ g/cm^3	
ion	ΔE^{solv}	$-T\Delta S^{solv}$	ΔE^{solv}	$-T\Delta S^{solv}$	ΔE^{solv}	$-T\Delta S^{solv}$
Cl^-	−71.5	0.8	−58.4	6.16	−56.5	6.32
OH^-	−98.3	5.0	−76.5	6.53	−69.0	6.28

$$\Delta E^{solv} = \Delta E^{solv}_{SW} + \Delta E^{solv}_{WW} \tag{16}$$

and

$$\Delta S^{solv} = \Delta S^{solv}_{SW} + \Delta S^{solv}_{WW} = \Delta S^{solv}_{SW} + \Delta E^{solv}_{WW}/T \tag{17}$$

ΔE^{solv} and ΔS^{solv} can be obtained from

$$\Delta E^{solv} = \left(\frac{\partial(\beta \Delta A^{solv}_S)}{\partial \beta}\right)_V \tag{18}$$

and

$$\Delta S^{solv} = k_B \beta^2 \left(\frac{\partial(\Delta A^{solv}_S)}{\partial \beta}\right)_V \tag{19}$$

with $\beta = 1/k_B T$ and ΔA^{solv}_S is the solvation free energy for solute S as defined by eq 1. The first terms in eqs 16 and 17 arise from different combinations of the ensemble average energy of the solute−solvent interactions. The second term in eqs 16 and 17 is sometimes called the solvent reorganization energy and is the difference of the average solvent−solvent interaction energy with and without the presence of the solute. This term is not zero even for infinitely dilute solutions[59,67,68] and can significantly contribute to the energies and entropies of solvation, but the resulting free energy clearly does not contain this term. When these properties are calculated from simulations, they are usually obtained from eqs 18 and 19 through numerical differentiations of the free energy with respect to temperature. Although only the first terms are truly direct "solvation" contributions, the second term cannot be ignored. This issue is important particularly in regions of large solvent compressibility, where the magnitude of ΔE^{solv}_{WW} becomes very large.

In Table 5 we report simulation results for changes in energy and entropy of solvation obtained by a thermodynamic perturbation method based on finite differences for the derivatives with respect to temperature.[69] It is well-known that the method has large statistical uncertainties associated with it; however, it is useful for determining qualitative trends by comparing the results under different conditions of the solvent. For ions, the solvation process is dominated by the energetic contribution. This is in contrast with the solvation of neutral molecules.[41,68,70] From Table 5 we can observe that the energetic contribution for both anions is negative and large, and the magnitude decreases when

TABLE 6: Calculated and Experimental Values of the Helmholtz Solvation Energy for NaCl in SCW

			ΔA^{solv} (kcal/mol)					ΔA^{solv} (kcal/mol)	
temp (K)	press. (bar)	density (g/cm^3)	exp[20]	simulation	temp (K)	press. (bar)	density (g/cm^3)	exp[20]	simulation ΔA^{solv} (kcal/mol)
673	300	0.29	−95.0	−126	768	50	0.0145	−33.7	−51.2
768	550	0.29	−79.2	−122	900	60	0.0145	−29.7	−52.5

TABLE 7: Estimated Contributions of First and Outer Shells to the Solvation Free Energies (kcal/mol)

ion	$T = 298$ K, $\rho = 0.997$ g/cm^3	$T = 673$ K, $\rho = 0.290$ g/cm^3	$T = 673$ K, $\rho = 0.087$ g/cm^3	$T = 768$ K, $\rho = 0.290$ g/cm^3
Cl^-				
total	−70.7	−52.2	−50.2	−48.6
first shell	−29.7 (4 Å)	−23.7 (4.75 Å)	−32.2 (4.75 Å)	−21.1 (4.75 Å)
outer shells	−40.9	−28.5	−17.9	−27.4
OH^-				
total	−93.3	−70.0	−62.7	−65.1
first shell	−46.5 (3.5 Å)	−36.1 (4 Å)	−41.4 (4 Å)	−32.5 (4 Å)
outer shells	−46.9	−33.9	−21.4	−32.6
Na^+				
total	−76.7	−73.7	−75.5	−73.7
first shell	−16.0 (2.7 Å)	−29.3 (3.05 Å)	−47.5 (3.05 Å)	−31.0 (3.05 Å)
outer shells	−60.7	−44.4	−28.0	−42.7

temperature increases and when the density of the solvent decreases. Due to the ion-induced ordering, the entropic contribution to the free energy is always negative, opposing the solvation process. Although the value of ΔS decreases at the SCW states with respect to AW due to the decrease in electrostriction, the product $T\Delta S$ has a slight increase; however, it remains small compared to the energetic term at these conditions.

We have not found divergences in the calculated energies and entropies of solvation at near-critical conditions. It is likely that the small size of our simulated system does not allow the critical fluctuations to grow as discussed by Guillot and Guissani.[68] On the other hand, calorimetric measurements for free energies, enthalpies, and entropies of solvation for NaCl and $CuCl_2$ solutions in water from room temperature to about 573 K[71] do show large changes in the magnitudes of the enthalpies and entropies of solvation when the temperature is increased at densities along the solvent coexistence curve near the critical point. These large changes reflect the contributions of the solvent reorganization terms in eqs 16 and 17, contrary to the explanation given[71] that the ion−solvent interaction energies become increasingly exothermic. The energetic and entropic solvent reorganization terms have opposite signs. Although they grow with density along the coexistence curve and for high temperatures near the critical point, they exactly cancel in the Helmholtz free energy.

5.2.3. Comparison to Experiments and Semicontinuum Models. In order to compare the simulation data with experiment, the ΔA^{solv} of NaCl has been determined by adding the single ion solvation energies from Table 4 (see Table 6). The experimental[20] ΔA^{solv} is determined from $\Delta G^{solv} - P\Delta V^{solv}$. The differences between simulation and experiment are likely caused by the same reasons cited above with regard to Sr^{2+}, including changes from infinite dilution to finite concentration and the limitations of our model. For example, ion pairing, which is not included in the model, decreases the magnitude of ΔA^{solv}, as shown in Table 6.

The high coordination numbers for SCW about ions were anticipated in semicontinuum models that were formulated before simulation data became available. In these semicontinuum models of ion hydration, the inner shell solvation was determined from gas-phase mass spectrometry data and the outer shell solvation from the Born equation.[20,22,72] Simulation data may be used to evaluate this simple yet powerful approach. To do this, we divide the total free energy into two terms:

$$\Delta A^{solv} = \Delta A^{solv}(\text{first shell}) + \Delta A^{solv}(\text{outer shells}) \quad (20)$$

where the total free energy comes from the simulation values listed in Table 4. In parallel with the semicontinuum models, the contribution of the outer shells is estimated by using the continuum Born model for a spherical ion. The radius is taken to be the distance corresponding to the minimum after the first shell in the solute−water pair radial distribution function. The dielectric constant used comes from Neumann's results for SPC/E water.[73] As shown in Table 7, the estimated contribution of the first shell, obtained by difference from eq 20, is roughly half of the total free energy (slightly less for Cl^-) for AW and dense SCW. The effect of temperature at constant density is small. The first shell becomes the major contributor to the total free energy as the water density is lowered. For example at $\rho = 0.087$ g/cm^3 and $T = 673.15$ K (Table 7), the first shell accounts for roughly two-thirds of the total free energy. This remarkable first shell solvation effect persists to extreme conditions where eventually the first shell starts to desolvate. For the chloride ion, from previous simulation studies[30,31] we have found that this threshold for desolvation occurs only at very low densities and relatively high temperatures. In this work we have performed a similar analysis for Na^+ (Figure 8), leading to an even higher temperature value for the threshold compared to Cl^-.

TABLE 8: ΔA^{solv} (First Shell) in kcal/mol Estimated from Models and Simulations at 300 bar ($\rho = 0.29$ g/cm^3) and 673 K

ion	Gupta and Johnston's model [22]	Tanger and Pitzer's model [20]	simulations (this work)
Cl^-	−23. 2	−19.2	−23.6
Na^+	−45.9	−41.3	−29.3

The results from Table 7 provide some justification for the semicontinuum models[20,22] in that outer-shell contributions to the solvation free energy dominate the region of higher densities while inner shells are more important at low densities. A comparison of ΔA^{solv} (first shell) obtained from the simulations using eq 20 with the results from the Tanger and Pitzer[20] and Gupta and Johnston[22] models is presented in Table 8 for Cl^- and Na^+. For Cl^-, very good agreement is found with the semicontinuum model that includes H bonding.[22] For Na^+, both semicontinuum models predict a larger magnitude of the first

shell contribution with respect to simulation for reasons that are unknown. Also, the magnitude of the simulation value of ΔA^{solv} for Na^+ in AW (Table 4) is below the average experimental value (Table 3).

6. Conclusions

Free energies of solvation in SCW have been simulated for the first time and have been analyzed in terms of the solvation structure. Due to the strong nature of the ion−water interactions, high coordination numbers are found to persist in the first shell for anions and cations even at 768 K and a very low density of 0.087 g/cm^3. The degree of persistence in the solvation free energy, as well as the hydrogen bonds and other specific interactions (determined geometrically), follows the calculated solute−water pair energy distributions in the order $Na^+ > OH^- > Cl^- > H_2O > HCl$.

In the case of anions, a substantial part of the first-shell interaction is due to the formation of solute−water H bonds. Due to the large negative charge on the oxygen site, OH^- develops a stronger H bond than Cl^-, while the water−water H bond is weak and the easiest to break by thermal forces.

For cations, the interaction in the first shell is dominated by electrostatic forces between the cation and the negatively charged oxygen in the water molecule. The simulations show that this type of interaction is much less affected by temperature up to 1000 K than the anion−water H bonds. Therefore, for Na^+, a remarkable result is that the free energy of solvation hardly changes from 300 to 800 K, whereas it decreases by about 25% for the anions. The small size of Na^+ and strong interactions with water explain these differences in solvation. In addition, bivalent cations exhibit a well-defined second shell that remains at supercritical conditions. The simulated local densities for bivalent cations are overestimated when compared to recent experimental findings in SCW.[47] We attribute these discrepancies to some combination of differences in concentration (finite concentration versus infinite dilution), experimental uncertainties, and the simple form of the potential functions in the simulations. The same issues may explain discrepancies between the simulated and experimental values of the free energy of solvation of NaCl.

The neutral molecules water and HCl are included for comparison. The coordination number and consequently the solvation properties of neutral molecules decrease dramatically from AW to SCW. For these much weaker interactions, solvation is much more influenced by entropic effects, as opposed to the case of ions, where solvation is highly exothermic and dominated by energetic contributions.[41,68]

The simulations provide some justification for semicontinuum models[20,22,72] which explicitly described only inner shell solvation at a molecular level. In SCW, the reduction in total free energy is primarily due to the desolvation of the outer shells, especially at high temperatures and low densities.

The insight gained from the simulation, as well as the quantitative values, may be used to improve the development of molecular thermodynamic models and to design new microscopic and macroscopic laboratory experiments which will benefit the development of SCW processes. In particular, ion solvation is a key property for understanding various chemical reactions including acid−base reactions which are addressed in the following article in this issue.

Acknowledgments are made to the U.S. Army Research Office for University Research Initiative Grants DAAL 03-92-6-0174 and DAAH 04-93-6-0363 and to the Separations Research Program at the University of Texas. Partial support of this work by a grant from the R. A. Welch Foundation (F-0761) to P.J.R. is also acknowledged. We thank the University of Texas System Center for High Performance Computing and Cray Research Inc. for computational support. Partial support of this work was also provided by the Army Research Office Contract DAAL 03-89-C-0038 with the University of Minnesota Army High Performance Computing Research Center (AHPCRC) and the DoD Shared Resource Center at the AHPCRC. P.B.B. thanks Dr. Gabriela S. Del Buono for helpful discussions.

References and Notes

(1) Bockris, J. O. M.; Reddy, A. K. N. *Modern Electrochemistry*; Plenum Press: New York, 1970; Vol. 1.

(2) Friedman, H. L.; Krishnan, C. V. Thermodynamics of ion hydration. In *Water: A Comprehensive Treatise*; Franks, F., Ed.; Plenum Press: New York, 1973; Vol. 3, pp 1−118.

(3) Robinson, R. A.; Stokes, R. H. *Electrolyte Solutions*, 2nd ed.; Butterworths: London, 1959.

(4) Marcus, Y. *Ion Solvation*; John Wiley and Sons: Chichester, UK, 1985.

(5) Pitzer, K. S. *Activity Coefficients in Electrolyte Solutions*, 2nd ed.; CRC Press: Boca Raton, FL, 1991.

(6) Fernández-Prini, R. J.; Corti, H. R.; Japas, M. L. *High-Temperature Aqueous Solutions: Thermodynamic Properties*; CRC Press: Boca Raton, FL, 1992.

(7) Shaw, R. W.; Brill, T. B.; Clifford, A. A.; Eckert, C. A.; Franck, E. U. *Chem. Eng. News* **1991**, *69*, 26-39.

(8) Tester, J. W.; Holgate, H. R.; Armellini, F. J.; Webley, P. A.; Killilea, W. R.; Hong, G. T.; Barner, H. E. Supercritical Water Oxidation Technology: A Review of Process Development and Fundamental Research. In *Emerging Technologies in Hazardous Waste Management III*; Tedder, D. W., Pohland, F. G., Eds.; American Chemical Society: Washington, DC, 1993; Vol. 518, pp 35−76.

(9) Wood, R. H.; Smith-Magowan, D. In *Thermodynamics of Aqueous Systems with Industrial Applications*; Newman, S. A., Ed.; American Chemical Society: Washington, DC, 1980; Vol. 133, pp 569−581.

(10) Marshall, W. L.; Frantz, J. D. In *Hydrothermal Experimental Techniques*; Ulmer, G. C., Barnes, H. L., Eds.; John Wiley and Sons: New York, 1987; Chapter 11.

(11) Mesmer, R. E.; Sweeton, F. H.; Hitch, B. F.; Baes, C. F. In *High Temperature High Pressure Electrochemistry in Aqueous Solutions*; Jones, D. d. G., Staehle, R. W., Eds.; National Association of Corrosion Engineers: Houston, TX, 1976; pp 365−374.

(12) Helgeson, H. C.; Kirkham, D. H. *Am. J. Sci.* **1974**, *274*, 1089−1198.

(13) Helgeson, H. C.; Kirkham, D. H. *Am. J. Sci.* **1974**, *274*, 1199−1261.

(14) Helgeson, H. C.; Kirkham, D. H. *Am. J. Sci.* **1976**, *276*, 97−240.

(15) Helgeson, H. C.; Kirkham, D. H.; Flowers, G. C. *Am. J. Sci.* **1981**, *281*, 1249−1516.

(16) Shock, E. L.; Oelkers, E. H.; Johnson, J. W.; Sverjensky, D. A.; Helgeson, H. C. *J. Chem. Soc., Faraday Trans.* **1992**, *88*, 803−826.

(17) Pitzer, K. S. *J. Phys. Chem.* **1983**, *87*, 1120−1125.

(18) Pitzer, K. S.; Pabalan, R. T. *Geochim. Cosmochim. Acta* **1986**, *50*, 1445−1454.

(19) Rosseinsky, D. R. *Chem. Rev.* **1965**, *65*, 467−490.

(20) Tanger, J. C., IV; Pitzer, K. S. *J. Phys. Chem.* **1989**, *93*, 4941−4951.

(21) Born, M. *Z. Phys.* **1920**, *1*, 45−48.

(22) Gupta, R. B.; Johnston, K. P. *Ind. Eng. Chem. Res.* **1994**, *33*, 2819−2829.

(23) Wood, R. H.; Quint, J. R.; Grolier, J.-P. E. *J. Phys. Chem.* **1981**, *85*, 3944−3949.

(24) Flarsheim, W. M.; Bard, A. J.; Johnston, K. P. *J. Phys. Chem.* **1989**, *93*, 4234.

(25) Gilson, M. K.; Honig, B. *Proteins* **1988**, *4*, 7−18.

(26) Nicholls, A.; Sharp, K. A.; Honig, B. *Proteins* **1991**, *11*, 281−296.

(27) Tucker, S. C.; Gibbons, E. M. Theoretical Models of Anisole Hydrolysis in Supercritical Water: Understanding the Effects of Pressure on Reactivity. In *Structure and Reactivity in Aqueous Solution: Characterization of Chemical and Biological Systems*; Truhlar, D. G., Cramer, C. J., Eds.; American Chemical Society: Washington, DC, 1994; Vol. 568, pp 196−211.

(28) Bennett, G. E.; Johnston, K. P.; Rossky, P. J. *J. Phys. Chem.* **1995**, *99*, 16136−16143.

(29) Balbuena, P. B.; Johnston, K. P.; Rossky, P. J. *J. Am. Chem. Soc.* **1994**, *116*, 2689−2690.

(30) Balbuena, P. B.; Johnston, K. P.; Rossky, P. J. *J. Phys. Chem.* **1995**, *99*, 1554−1565.

(31) Flanagin, L. W.; Balbuena, P. B.; Johnston, K. P.; Rossky, P. J. *J. Phys. Chem.* **1995**, *99*, 5196−5205.
(32) dePablo, J. J.; Prausnitz, J. M.; Strauch, H. J.; Cummings, P. T. *J. Chem. Phys.* **1990**, *93*, 7355−7359.
(33) Guissani, Y.; Guillot, B. *J. Chem. Phys.* **1993**, *98*, 8221−8235.
(34) Mountain, R. D. *J. Chem. Phys.* **1989**, *90*, 1866−1870.
(35) Kalinichev, A. G.; Heinzinger, K. *Computer Simulations of Aqueous Fluids at High Temperatures and Pressures*; Springer-Verlag: New York, 1992.
(36) Cummings, P. T.; Chialvo, A. A.; Cochran, H. D. *Chem. Eng. Sci.* **1994**, *49*, 2735−2748.
(37) Cummings, P. T.; Cochran, H. D.; Simonson, J. M.; Mesmer, R. E.; Karaborni, S. *J. Chem. Phys.* **1991**, *94*, 5606−5621.
(38) Cochran, H. D.; Cummings, P. T.; Karaborni, S. *Fluid Phase Equilib.* **1992**, *71*, 1−16.
(39) Seminario, J. M.; Concha, M. C.; Murray, J. S.; Politzer, P. *Chem. Phys. Lett.* **1994**, *222*, 25−32.
(40) Gao, J. *J. Am. Chem. Soc.* **1993**, *115*, 6893−6895.
(41) Johnston, K. P.; Balbuena, P. B.; Xiang, T.; Rossky, P. J. Simulation and Spectroscopy of Solvation in Water from Ambient to Supercritical Conditions. In *Innovations in Supercritical Fluids*; Hutchenson, K. W., Foster, N. R., Eds.; American Chemical Society: Washington, DC, 1995; Vol. 608, pp 77−92.
(42) Gao, J. *J. Phys. Chem.* **1994**, *98*, 6049−6053.
(43) Cui, S. T.; Harris, J. G. *Chem. Eng. Sci.* **1994**, *49*, 2749−2763.
(44) Zwanzig, R. W. *J. Chem. Phys.* **1954**, *22*, 1420−1426.
(45) Mezei, M.; Beveridge, D. L. Free energy simulations. In *Annals New York Academy of Sciences*; Beveridge, D., Jorgensen, W. L., Eds.; New York Academy of Sciences: New York, 1986; Vol. 482, pp 1−23.
(46) Berendsen, H. J. C.; Grigera, J. R.; Straatsma, T. P. *J. Phys. Chem.* **1987**, *91*, 6269−6271.
(47) Pfund, D. M.; Darab, J. G.; Fulton, J. L.; Ma, Y. *J. Phys. Chem.* **1994**, *98*, 13102−13107.
(48) Ben-Naim, A. *Solvation Thermodynamics*; Plenum Press: New York, 1987.
(49) Frank, H. S. *J. Chem. Phys.* **1955**, *23*, 2023−2032.
(50) van Gunsteren, W. F.; Beutler, T. C.; Fraternali, F.; King, P. M.; Mark, A. E.; Smith, P. E. Computation of free energy in practice: Choice of approximations and accuracy limiting factors. In *Computer Simulation of Biomolecular Systems*; vanGunsteren, W. F., Weiner, P. K., Wilkinson, A. J., Eds.; ESCOM Science Publishers: Leiden, The Netherlands, 1993; Vol. 2, pp 315−348.
(51) de Leeuw, S. W.; Perram, J. W.; Smith, E. R. *Proc. R. Soc. London* **1980**, *A373*, 27−56.
(52) Belhadj, M.; Alper, H. E.; Levy, R. M. *Chem. Phys. Lett.* **1991**, *179*, 13−20.
(53) Pearlman, D. A. *J. Phys. Chem.* **1994**, *98*, 1487−1493.
(54) Wood, W. W. In *Physics of Simple Liquids*; North-Holland: Amsterdam, 1968.
(55) Berendsen, H. J. C.; Postma, J. P. M.; van Gunsteren, W. F.; Hermans, J. *Intermolecular Forces*; Reidel: Dordrecht, 1981.
(56) DelBuono, G. S.; Rossky, P. J.; Schnitker, J. *J. Chem. Phys.* **1991**, *95*, 3728.
(57) Aqvist, J. *J. Phys. Chem.* **1990**, *94*, 8021−8024.
(58) Geiger, A. *Ber. Bunsen-Ges. Phys. Chem.* **1981**, *85*, 52−63.
(59) Yu, H.-A.; Karplus, M. *J. Chem. Phys.* **1988**, *89*, 2366−2379.
(60) Bergström, P.-A.; Lindgren, J.; Read, M.; Sandström, M. J. *J. Phys. Chem.* **1991**, *95*, 7650−7655.
(61) Lindgren, J.; Hermansson, K.; Wójcik, M. J. *J. Phys. Chem.* **1993**, *97*, 5254−5259.
(62) Danielewicz-Ferchmin, I. *J. Phys. Chem.* **1995**, *99*, 5658−5665.
(63) Balbuena, P. B.; Johnston, K. P.; Rossky, P. J. To be published.
(64) Madura, J. D.; Jorgensen, W. L. *J. Am. Chem. Soc.* **1986**, *108*, 2517−2527.
(65) Chandrasekhar, J.; Smith, S. F.; Jorgensen, W. L. *J. Am. Chem. Soc.* **1985**, *107*, 154−163.
(66) Rashin, A. A.; Honig, B. *J. Phys. Chem.* **1985**, *89*, 5588−5593.
(67) Garisto, F.; Kusalik, P. G.; Patey, G. N. *J. Chem. Phys.* **1983**, *79*, 6294−6300.
(68) Guillot, B.; Guissani, Y. *J. Chem. Phys.* **1993**, *99*, 8075−8094.
(69) Fleischman, S. H.; Brooks, C. L., III. *J. Chem. Phys.* **1987**, *87*, 3029−3037.
(70) Franks, F. *Faraday Symp. Chem. Soc.* **1982**, *17*, 7−10.
(71) Cobble, J. W.; Murray, R. C., Jr. *Faraday Discuss. Chem. Soc.* **1977**, *64*, 144−149.
(72) Smits, P. J.; Economou, I. G.; Peters, C. J.; Arons, J. d. S. *J. Phys. Chem.* **1994**, *98*, 12080−12085.
(73) Neumann, M. Computer Simulation of Water and The Dielectric Equation of State. Presented at the 12th International Conference on the Properties of Water and Steam, Orlando, FL, 1994.
(74) Weiner, S. J.; Kollman, P. A.; Nguyen, D. T.; Case, D. A. *J. Comput. Chem.* **1986**, *7*, 230−252.
(75) Chandrasekhar, J.; Spellmeyer, D. C.; Jorgensen, W. L. *J. Am. Chem. Soc.* **1984**, *106*, 903−910.
(76) Field, M. J.; Bash, P. A.; Karplus, M. *J. Comput. Chem.* **1990**, *11*, 700−733.
(77) Rao, B. G.; Singh, U. C. *J. Am. Chem. Soc.* **1990**, *112*, 3803−3811.
(78) Salomon, M. *J. Phys. Chem.* **1970**, *74*, 2519−2524.
(79) Pearson, R. G. *J. Am. Chem. Soc.* **1986**, *108*, 6109−6114.

JP952194O